

# Dirac Coupled Channel Analyses of Proton Inelastic Scattering from $^{40}\text{Ar}$ Nucleus

Sugie Shim\*

*Department of Physics, Kongju National University, Gongju 314-701*

(Received 2015)

## Abstract

0.8 GeV proton inelastic scatterings from  $^{40}\text{Ar}$  nucleus are analyzed using an optical potential model in the Dirac coupled channel formalism. A rotational collective model is used to obtain the transition optical potentials for the low lying excited states of the rotational band. The optical potential parameters of a Woods-Saxon shape and the deformation parameters of the excited states are searched phenomenologically to reproduce the experimental differential cross-section data by using the sequential iteration method. The effect of a multistep process is investigated by including the channel coupling between two excited states in addition to the couplings between the ground state and the excited states. The calculated deformation parameters of the excited states are compared with those obtained by using the nonrelativistic calculations. The results of the Dirac coupled channel calculations are found to show pretty good agreements with the experimental data of the ground state and the low-lying excited states. The multistep excitation process via the channel coupling with the second  $2^+$  state is found to be important for the excitation of the  $4^+$  state at the inelastic scatterings from the deformed nucleus,  $^{40}\text{Ar}$ .

PACS numbers: 25.40.Ep, 24.10.Jv, 24.10.Ht, 24.10.Eq, 21.60.Ev

Keywords: Dirac phenomenology, Coupled channel calculation, Optical potential model, Collective model, Proton inelastic scattering

---

\*Electronic address: shim@kongju.ac.kr; Fax: +82-41-850-8489

## I. INTRODUCTION

Relativistic approaches based on the Dirac equation as the relevant wave equation have proved to be very successful in treating the proton elastic and inelastic scatterings at intermediate energies from the spherically symmetric nuclei [1-4] and a few deformed nuclei [5-12]. Considerable improvements have been shown in the coupled channel calculations using the Dirac phenomenology compared to the classical nonrelativistic calculations based on the Schrödinger equation [8-13].

In this work we use phenomenological optical potentials in the Dirac coupled channel calculation [1,2] to analyze 0.8 GeV proton inelastic scatterings from a deformed nucleus,  $^{40}\text{Ar}$ . So far only the distorted wave Born approximation (DWBA) calculation using phenomenological optical potentials in nonrelativistic formalism neglecting the coupled channel effects, or the nonrelativistic coupled channel calculation at low energy has been done to analyze the inelastic scatterings of proton from  $^{40}\text{Ar}$  nucleus [14, 15]. A rotational collective model is used for the transition optical potentials to accommodate the collective motion of excited deformed nuclei considering the low lying excited states of the rotational bands [5]. The multistep excitation process is included in the calculation by considering the coupling between two excited states, in addition to the couplings between the ground and the excited states. In order to solve the complicated Dirac coupled channel equations, we use a computer program called ECIS [16] where the Dirac optical potential and the deformation parameters are determined phenomenologically by using a sequential iteration method. The Dirac equations are reduced to Schrödinger-like second-order differential equations to obtain the effective central and spin-orbit optical potentials, and the obtained effective potentials are analyzed and compared with those of the nonrelativistic calculations. The calculated deformation parameters for the low-lying excited states of the  $^{40}\text{Ar}$  nucleus are analyzed and compared with those calculated by using the nonrelativistic approaches.

## II. THEORY AND RESULTS

Dirac analyses are performed phenomenologically for 0.8 GeV unpolarized proton inelastic scatterings from  $^{40}\text{Ar}$  nucleus by using an optical potential model and a collective model. Because  $^{40}\text{Ar}$  is a spin-0 nucleus, only scalar, time-like vector and tensor optical potentials

survive [17, 18], as in spherically-symmetric nuclei; hence, the relevant Dirac equation for the elastic scattering from the nucleus is given as

$$[\alpha \cdot p + \beta(m + U_S) - (E - U_V^0 - V_c) + i\alpha \cdot \hat{r}\beta U_T]\Psi(r) = 0. \quad (1)$$

Here,  $U_S$  is a scalar potential,  $U_V^0$  is a time-like vector potential,  $U_T$  is a tensor potential, and  $V_c$  is the Coulomb potential. Even though tensor potentials always present due to the interaction of the anomalous magnetic moment of the projectile with the charge distribution of the target, they have been found to be always very small compared to the scalar or the vector potentials [2]. Hence they are neglected in this calculation. The scalar and the vector optical potentials are complex, and have the Woods-Saxon shapes [13] as they are assumed to follow the distribution of the nuclear density. In the first-order rotational model of ECIS, the deformation of the radius of the optical potential is given by using the Legendre polynomial expansion method [13]. We assume that the shapes of the deformed potentials follow the shapes of the deformed nuclear densities and that the transition potentials can be obtained by assuming that they are proportional to the first-order derivatives of the diagonal potentials. However, depending on the model assumed, pseudo-scalar and axial-vector potentials may also be present in the equation when we consider the inelastic scattering. In the collective model approach used in this work, we assume that we can obtain appropriate transition potentials by deforming the direct potentials that describe the elastic channel reasonably well [19]. The transition potentials are given by

$$U_S^\lambda(r) = \frac{\beta_S^\lambda}{(2\lambda + 1)^{1/2}} \left[ R_S^r \frac{d(\text{Re}U_S(r))}{dR_S^r} + iR_S^i \frac{d(\text{Im}U_S(r))}{dR_S^i} \right] Y_{\lambda 0}^*(\Omega), \quad (2)$$

$$U_V^{0,\lambda}(r) = \frac{\beta_V^\lambda}{(2\lambda + 1)^{1/2}} \left[ R_V^r \frac{d(\text{Re}U_V^0(r))}{dR_V^r} + iR_V^i \frac{d(\text{Im}U_V^0(r))}{dR_V^i} \right] Y_{\lambda 0}^*(\Omega), \quad (3)$$

where  $\lambda$  is the multipolarity, superscripts  $r$  and  $i$  refer to the real and the imaginary parts of the radius ( $R$ ) parameters. The real and the imaginary  $\beta_\lambda$  are taken to be equal for a given potential type, so that  $\beta_S$  and  $\beta_V$  are determined for each excited state. The Dirac coupled channel equations are solved numerically using the computer code ECIS [16] which employs the sequential iteration method. We consider both the couplings between the  $0^+$  ground state and the low lying excited states and also coupling between two excited states, for example, between the  $2^+$  and the  $4^+$  states. Hence the multistep process is included in the calculation. Because the channel couplings between the low-lying excited states of the

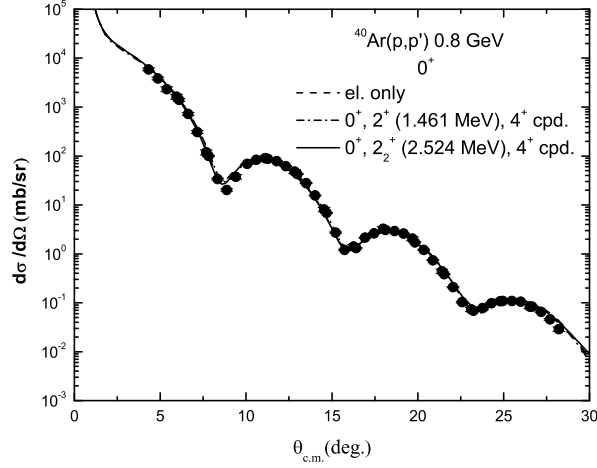


FIG. 1: Differential cross section of the ground state for 0.8 GeV  $p + {}^{40}\text{Ar}$  scattering. The dashed, the dash-dot and the solid lines represent the results of Dirac phenomenological calculations where only the ground state is considered, where the ground, the first  $2^+$  (1.461 MeV) and the  $4^+$  states are coupled, and where the ground, the second  $2^+$  (2.524 MeV) and the  $4^+$  states are coupled, respectively.

rotational band are strong in the inelastic scatterings from a deformed nucleus, the multistep transition process could be important. In order to compare the calculated results with those of nonrelativistic calculations, we reduce the Dirac equation to a Schrödinger-like second-order differential equation by considering the upper component of the Dirac wave function and obtain the effective central and spin-orbit optical potentials [2].

The elastic and inelastic data are obtained from Ref. 14 for 0.8 GeV proton inelastic scatterings from  ${}^{40}\text{Ar}$  nucleus. The low lying excited states of the  $2^+$  (1.461 MeV),  $2^+$  (2.524 MeV) and  $4^+$  (2.89 MeV) are considered and assumed to be collective rotational states in the calculation. The 12 parameters of the diagonal scalar and vector optical potentials in the Woods-Saxon shapes are obtained by fitting the elastic scattering data. Pretty good agreements with the elastic scattering data are obtained as shown by the dashed lines in Fig. 1. For the inelastic scattering calculations, we include only the ground and one excited states at once in the calculations as a first step. Next, the ground, the first  $2^+$  or the second  $2^+$ , and  $4^+$  states are included in the calculations to investigate the effect of the channel coupling between the excited states.

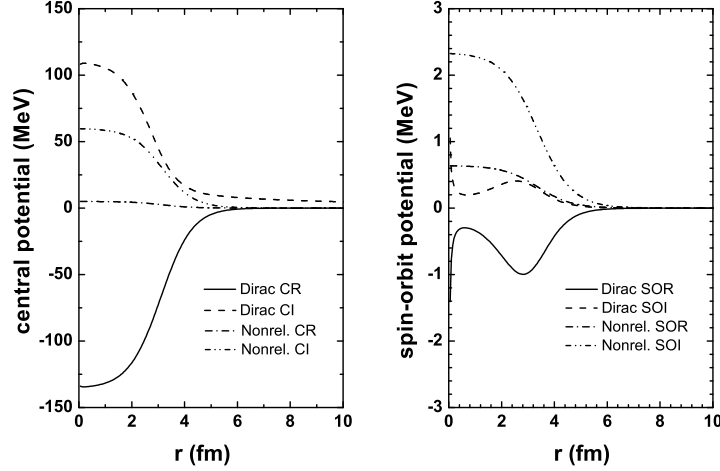


FIG. 2: Comparison of the Dirac effective central and spin-orbit potentials of  $^{40}\text{Ar}$  with those of the nonrelativistic (Nonrel.) calculations. CR, CI, SOR and SOI mean central real, central imaginary, spin-orbit real, and spin-orbit imaginary potentials, respectively.

TABLE I: Calculated phenomenological optical potential parameters of a Woods-Saxon shape for 0.8 GeV proton elastic scatterings from  $^{40}\text{Ar}$  nucleus.

Potential	Strength (MeV)	Radius (fm)	Diffusiveness (fm)
Scalar	-472.8	3.154	0.5967
real			
Scalar	120.3	3.013	0.6896
imaginary			
Vector	264.0	3.153	0.5954
real			
Vector	-127.3	3.129	0.6254
imaginary			

The calculated optical potential parameters of the Woods-Saxon shape for 0.8 GeV proton elastic scatterings from  $^{40}\text{Ar}$  nucleus are shown in Table 1.  $\chi^2/N$ , where  $N$  is the number of experimental data, is about 13.4. We observe that the real parts of the scalar potentials and the imaginary parts of the vector potentials turn out to be large and negative and that

the imaginary parts of the scalar potentials and the real parts of the vector potentials turn out to be large and positive, showing the same pattern as in spherically-symmetric nuclei [2–4].

In Fig. 2, the Dirac effective central and spin-orbit potentials for  $^{40}\text{Ar}$  are compared with those of the nonrelativistic calculations [14]. We should note that one of the merits of using the relativistic approach based on the Dirac equation instead of using the nonrelativistic approach based on the Schrödinger equation is that the spin-orbit potential appears naturally in the Dirac approach when the Dirac equation is reduced to a Schrödinger-like second-order differential equation, whereas the spin-orbit potential must be inserted by hand in the nonrelativistic Schrödinger approach. The surface-peaked phenomena observed for most of the s-d shell deformed nuclei [7, 10–13] are not observed at the effective central potentials when  $^{40}\text{Ar}$  nucleus is considered. The strength of the real effective central potential of the Dirac approach turns out to be large, about -130 MeV at the center of the nucleus, compared to that of the nonrelativistic Schrödinger approach, which is about 4.0 MeV [14]. The real parts of the effective central and spin-orbit potentials turn out to have negative values as in the cases of the other deformed nuclei [12, 13], while those of the nonrelativistic calculations are found to have positive values. Surface-peaked phenomena are clearly shown at the effective spin-orbit potentials, indicating that the spin-orbit interaction is a surface-peaked interaction. The surface-peaked shape cannot be obtained in the conventional nonrelativistic calculations because the Woods-Saxon shape is used for both the central and the spin-orbit potentials, as shown in the figure.

Next, six-parameter searches are performed by including one excited state in addition to the ground state, starting from the 12 parameters obtained for the direct optical potentials in the elastic scattering calculation. Here, six parameters are the two deformation parameters,  $\beta_S$  and  $\beta_V$ , for the each excited state and the four potential strengths, the scalar real and imaginary potential strengths and the vector real and imaginary potential strengths, keeping the potential geometries unchanged. The optical potential strengths obtained by fitting the elastic scattering data in the elastic scattering calculation are varied because the channel coupling of the excited states to the ground state should be included in the inelastic scattering calculation. Finally, eight-parameter searches are performed by considering three states, the ground, the first  $2^+$  or the second  $2^+$  state, and the  $4^+$  states, together in the calculation in order to investigate the effect of the channel coupling between the excited

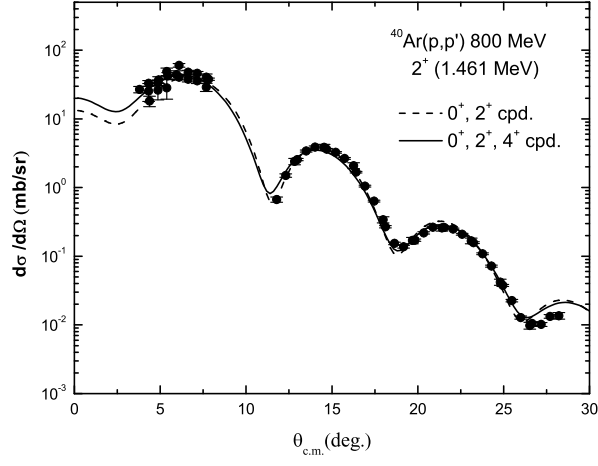


FIG. 3: Differential cross section of the first  $2^+$  state (1.461 MeV) for 0.8 GeV  $p + {}^{40}\text{Ar}$  inelastic scattering. The dashed and the solid lines represent the results of Dirac coupled channel calculations where the ground and the first  $2^+$  states are coupled and where the ground, the first  $2^+$  and the  $4^+$  states are coupled, respectively.

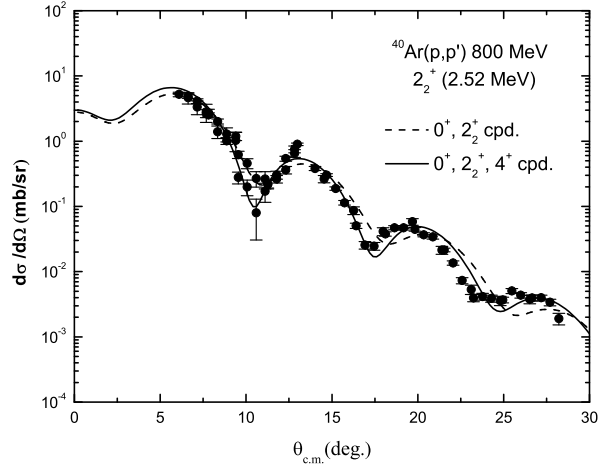


FIG. 4: Differential cross section of the second  $2^+$  state (2.524 MeV) for 0.8 GeV  $p + {}^{40}\text{Ar}$  inelastic scattering. The dashed and the solid lines represent the results of Dirac coupled channel calculations where the ground and the second  $2^+$  states are coupled and where the ground, the second  $2^+$  and the  $4^+$  states are coupled, respectively.

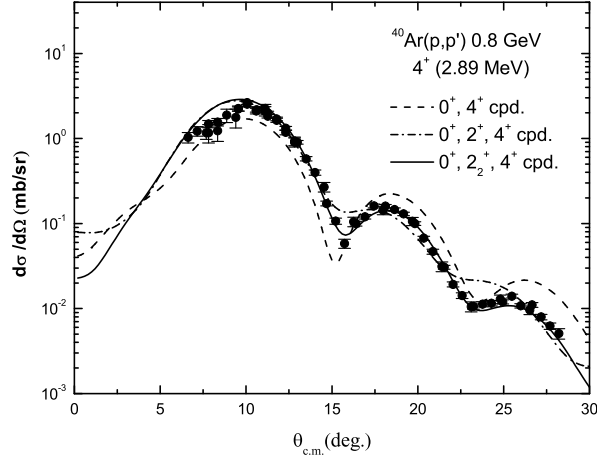


FIG. 5: Differential cross section of the  $4^+$  state for 0.8 GeV  $p + {}^{40}\text{Ar}$  inelastic scattering. The dashed, the dash-dot and the solid lines represent the results of Dirac coupled channel calculations where the ground and the  $4^+$  states are coupled, where the ground, the first  $2^+$  and the  $4^+$  states are coupled, and where the ground, the second  $2^+$  and the  $4^+$  states are coupled, respectively.

states, and the results are compared with those obtained by the calculation where only the ground and one excited states are coupled. Figure 1 shows the results of the coupled channel calculations for the ground state, showing about the same pretty good agreements with the experimental elastic differential cross section data in all the cases. In the figures, ‘cpd’ means ‘coupled’. In Figs. 3, 4 and 5, the calculated observables for the first  $2^+$ , the second  $2^+$ , and the  $4^+$  states are compared with the experimental data. For the first  $2^+$  state, the agreements with the experimental data are pretty good even when only the ground and the first  $2^+$  states are coupled as shown by the dashed lines in Fig. 3. The agreements with the experimental data are not changed much by adding the coupling with the  $4^+$  state, as shown by the solid lines.  $\chi^2/N$  for the two cases turns out to be about the same. The agreements with the experimental data for the  $4^+$  state are not good when only the ground and the  $4^+$  states are coupled, as shown by the dashed lines in Fig. 5 and they are not improved much by adding the coupling with the first  $2^+$  state, as shown by the dash-dot lines. However, the agreements with the experimental data for the  $4^+$  state are improved significantly by adding the coupling with the second  $2^+$  state, as shown by the solid lines in Fig. 5, indicating that the multistep excitation process via the channel coupling with



the second  $2^+$  state is important for the excitation of the  $4^+$  state. The agreements with the experimental data for the second  $2^+$  state are also improved noticeably by adding the coupling with the  $4^+$  state, as shown by the solid lines in Fig. 4. Hence the multistep transition process is confirmed to be important because the excited states of a rotational band, they are the second  $2^+$  and the  $4^+$  states in this case, are strongly coupled to each other, as shown previously for the inelastic scatterings from the other axially-symmetric deformed nuclei [10–13]. This is not the case for the spherically-symmetric nuclei, where the excited states are well described by considering the coupling via single-step transitions [2, 3]. Even though the results of the Dirac coupled channel calculation show pretty good agreements with the second  $2^+$  data, the second and the third minima of the diffraction pattern are found to be shifted slightly from the data. This slight discrepancy could be due to the coupling effect of the second  $2^+$  state with the excited  $0^+$  state at 2.12 MeV, that is omitted in the calculation. Reproducing hadron scattering experimental data of excited  $0^+$  levels is known to be notoriously difficult because the form factors of  $\lambda = 0$  transitions, the assignment of the excited  $0^+$  state to a band structure, the reduced matrix elements, and the relative phases for all the multipolarities of the different transitions are not well known [15]. Hence the coupling to the excited  $0^+$  state is not included in the calculation, even though the excited  $0^+$  state, the second  $2^+$  state and the  $4^+$  state could form a  $\beta$  rotational band [14, 15] and coupled to each other. The potential strengths are changed to -185.1, 396.0, 117.8, and -264.6 MeV for the scalar real and imaginary and the vector real and imaginary potentials, respectively, in the first  $2^+$  state coupled case, to -479.1, 109.2, 273.3, and -122.6 MeV in the second  $2^+$  state coupled case, to -383.9, 302.8, 219.5, and -206.7 MeV in the  $4^+$  state coupled case, to -462.9, 191.9, 264.1, and -157.5 MeV in the first  $2^+$  and the  $4^+$  states coupled case, and to -502.3, 93.41, 283.2, and -114.4 MeV in the second  $2^+$  and the  $4^+$  states coupled case. The results of our relativistic coupled channel calculation show clearly better agreements with the experimental data than those of the nonrelativistic DWBA calculations [14].

In Table 2, we show the deformation parameters for the first  $2^+$ , the second  $2^+$  and the  $4^+$  excited states of  $^{40}\text{Ar}$  nucleus.  $\beta_S$  is observed to be always larger than  $\beta_V$  for the excited states that we considered in the calculations. The deformation parameters obtained from the Dirac phenomenological coupled channel calculation for the first  $2^+$ , the second  $2^+$  and the  $4^+$  excited states of  $^{40}\text{Ar}$  are found to show pretty good agreements with those obtained

TABLE II: Comparison of the deformation parameters for the first  $2^+$ , the second  $2^+$  and the  $4^+$  excited states for 0.8 GeV proton inelastic scatterings from  $^{40}\text{Ar}$  nucleus with those obtained by using the nonrelativistic calculations.

	Energy (MeV)	$\beta_S$	$\beta_V$	$\beta_{NR}$
$2^+$ state	1.461	.28	.27	.28 <sup>14</sup>
$2_2^+$ state	2.524	.085	.058	.082 <sup>14</sup>
$4^+$ state	2.89	.092	.057	.0935 <sup>14</sup>

by using the nonrelativistic DWBA calculations [14] using the same Woods-Saxon shapes for the geometries of the optical potentials, even though the theoretical bases are quite different.

### III. CONCLUSIONS

A relativistic Dirac coupled channel calculation using an optical potential model is able to describe the low-lying excited states of the rotational bands for 0.8 GeV unpolarized proton inelastic scatterings from a deformed nucleus  $^{40}\text{Ar}$  pretty well. The observables obtained by our relativistic coupled channel calculation show clearly better agreements with the experimental data than those obtained by the nonrelativistic DWBA calculations. The Dirac equations are reduced to second-order differential equations to obtain Schrödinger-equivalent effective central and spin-orbit potentials, and surface-peaked phenomena are observed only at the effective spin-orbit potentials for the scatterings from  $^{40}\text{Ar}$  nucleus. The first-order rotational collective models are used to describe the low-lying excited states of the rotational band in the nucleus, and the calculated deformation parameters are compared with those obtained by using the nonrelativistic calculations. The deformation parameters obtained from the Dirac phenomenological calculations for the first  $2^+$ , the second  $2^+$ , and the  $4^+$  state of  $^{40}\text{Ar}$  are found to show pretty good agreements with those obtained by using the nonrelativistic calculations. The agreements with the experimental data for the  $4^+$  state are not good when only the ground and the  $4^+$  states are coupled or when the ground, the first  $2^+$  and the  $4^+$  states are coupled. But they are improved significantly when the ground, the second  $2^+$  and the  $4^+$  states are coupled, indicating that the multistep excitation process

via the channel coupling with the second  $2^+$  state is important for the excitation of the  $4^+$  state for the inelastic scattering from the deformed nucleus,  $^{40}\text{Ar}$ .

- 
- [1] L. G. Arnold, B. C. Clark, R. L. Mercer, and P. Swandt, Phys. Rev. C **23**, 1949 (1981).
  - [2] S. Shim, Ph.D. dissertation, The Ohio State University 1989; L. Kurth, B. C. Clark, E. D. Cooper, S. Hama, S. Shim, R. L. Mercer, L. Ray, and G. W. Hoffmann, Phys. Rev. C **49**, 2086 (1994).
  - [3] S. Shim, B. C. Clark, S. Hama, E. D. Cooper, R. L. Mercer, L. Ray, and G. W. Hoffmann, Phys. Rev. C **38**, 1968 (1988).
  - [4] S. Shim, B.C. Clark, E.D. Cooper, S. Hama, R.L. Mercer, L. Ray, J. Raynal, and H.S. Sherif, Phys. Rev. C **42**, 1592 (1990).
  - [5] R. de Swiniarski, D. L. Pham, and J. Raynal, Phys. Lett. B **213**, 247 (1988).
  - [6] R. de Swiniarski, D. L. Pham, and J. Raynal, Z. Phys. A-Hadrons and Nuclei **343**, 179 (1992).
  - [7] D. L. Pham and R de Swiniarski, Nuovo Cimento A **107**, 1405 (1994).
  - [8] M. L. Barlett, J. A. McGill, L. Ray, M. M. Barlett, G. W. Hoffmann, N. M. Hintz, G. S. Kyle, M. A. Franey, and G. Blanpied, Phys. Rev. C, **22**, 1168 (1980).
  - [9] J. J. Kelly, Phys. Rev. C **71**, 064610 (2005).
  - [10] S. Shim, M. W. Kim, B. C. Clark, and L. Kurth Kerr, Phys. Rev. C **59**, 317 (1999).
  - [11] S. Shim, Shin-Ho Ryu and Min-Soo Kim, J. Korean. Phys. Soc. **51**, 271 (2007); S. Shim, Shin-Ho Ryu and Min-Soo Kim, J. Korean. Phys. Soc. **53**, 1146 (2008).
  - [12] S. Shim and M. W. Kim, Int. J. Mod. Phys. E **21**, 1250098 (2012).
  - [13] S. Shim and M. W. Kim, J. Korean. Phys. Soc. **64**, 483 (2014).
  - [14] G. S. Blanpied, B. G. Ritchie, M. L. Barlett, R. W. Ferguson, J. A. McGill, and B. H. Wildenthal, Phys. Rev. C **37**, 1304 (1988).
  - [15] R. De Leo, S. Micheletti, M. Pignanelli and M. N. Harakeh, Phys. Rev. C **31**, 362 (1985).
  - [16] J. Raynal, *Computing as a Language of Physics*, ICTP International Seminar Course, 281 (IAEA, Italy, 1972); J. Raynal, *Notes on ECIS94*, Note CEA-N-2772, 1994.
  - [17] R. J. Furnstahl, C. E. Price, and G. E. Walker, Phys. Rev. C **36**, 2590 (1987).
  - [18] L. Ray and G. W. Hoffmann, Phys. Rev. C **31**, 538 (1986).
  - [19] J. Raynal and H.S. Sherif, J. Phys. Soc. Jpn. Suppl. **55**, 992 (1985).